High-Temperature Oxidation Behaviour of High Entropy Alloys

Eddy Agus Basuki[1*], *Mohamad Ali* Akbar[1], *Ahmad Ade* Syabihis[1], *Tria Laksana* Ahmad[1], *Akhmad Ardian* Korda[1], *Fadhli* Muhammad[1], *Budi* Prawara[2], *Djoko Hadi* Prajitno[3], *Bagus Hayatul* Jihad[4] and *Muhamad Hananuputra* Setianto[4]

[1]Department of Metallurgical Engineering, Faculty of Mining and Petroleum Engineering, Bandung Institute of Technology
[2]Electronics and Informatics Research Organization, National Research and Innovation Agency (BRIN).
[3]Nuclear Research Centre, National Research and Innovation Agency (BRIN)
[4]Research Centre for Rocket Technology, Research Organization for Aeronautics and Space, National Research and Innovation Agency (BRIN).

Abstract. High-temperature operation, such as in gas turbine engines, is typically limited by the ability of materials to withstand extreme operating conditions. The need for a combination of high-temperature strength and oxidation resistance, as well as microstructural stability, has led to the continued use of nickel-based superalloys as materials for turbine blades, the most critical component in aero gas turbine engines. Due to their limited melting points, materials beyond superalloys are needed to meet increasing fuel efficiency requirements. High entropy alloys have recently been considered as candidates for materials to replace nickel-based superalloys. This paper discusses the microstructures and high-temperature oxidation behavior of $Al_{0.75}CoCrCuFeNi$ high entropy alloy at 900, 1000, and 1100°C. It was found that the oxidation rate constants for $Al_{0.75}CoCrCuFeNi$ oxidized at 900, 1000, and 1100°C are 3.84 x 10^{-10}, 5.99 x 10^{-10}, and 8.97 x 10^{-10} (mg/cm^2.s), respectively, with an activation energy for oxidation of 66.58 kJ/mol.

1 INTRODUCTION

The sustainability of the supply of engineering alloys to meet long-term global demand is a major concern and issue for many parties, including industry players, research and educational institutions, and governments. The main concerns range from the search for alternative renewable energy sources to the development of new high-performance materials. In particular, there is a growing need for engineering alloys with superior functional properties for long-life, high-temperature applications. The capability of aircraft turbine blades is limited to 1100°C for a 10,000-hour life, while nozzle rockets have relatively short lifetimes but require much higher temperatures of up to about 3000°C. The material properties required for high-temperature applications are as follows: the materials should have high melting points; high mechanical properties in terms of creep, toughness, and thermal fatigue; good high-temperature corrosion resistance; high microstructural stability; and easy for fabrication, such as casting, forging, powder metallurgy of additive manufacturing and welding.

Superalloys are a group of alloy materials that have been used for high-temperature applications [10]. These materials are classified as heat-resistant alloys based on nickel, iron-nickel, and cobalt with a combination of high strength and corrosion resistance at homologous temperatures higher than 0.6. The homologous temperature is defined as the ratio of the operating temperature to the melting temperature of the material ($\tau = T_{op}/T_m$). To date, nickel-based superalloys have been the most successful alloy systems for high-temperature applications. In today's aircraft jet engines, gas entry temperatures from the combustion chamber are higher and exceed the melting temperature of nickel-based superalloys, which is approximately 1450°C. In order to achieve higher fuel efficiency and lower CO_2 gas emissions, these materials are operating at turbine entry temperatures of approximately 1700°C through the use of advanced alloy systems, cooling systems, and thermal barrier coatings.

Nevertheless, at present nickel-based superalloys have reached their peak operating temperature close to the γ/γ' equilibrium solvus temperature, which is about 80% of their melting temperature, above which a complete dissolution of the γ' precipitate can occur, leaving a relatively weak matrix of γ solid solution. These ordered, coherent γ'-Ni_3(Al, Ti) precipitates play an important role as a primary strengthening agent alongside carbides and other intermetallic compounds, as shown in Fig. 1. To further improve energy efficiency and environmental friendliness based on thermodynamic principle, higher turbine entry temperatures are required. Since the development of nickel-based superalloys cannot be sustained indefinitely, alternative new materials beyond the temperature capabilities of Ni-based superalloys are required [6]. Several alloys have been investigated, *i.e.*, aluminide systems based on Ni, Fe, Co, Ti, and refractory elements such as Mo. The brittleness of such aluminide systems is the most critical challenge for these materials to replace Ni-based superalloys.

*Corresponding author: eddy.a.basuki@itb.ac.id

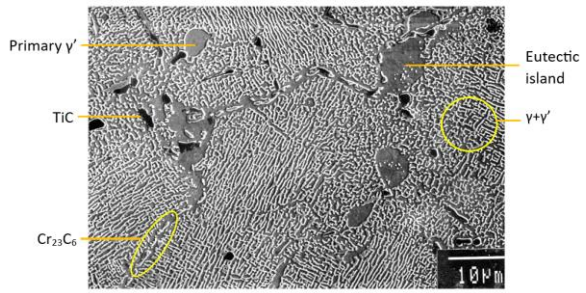

Fig. 1. A typical microstructure of the Ni-base single crystal superalloy with a γ/γ' coherent structure [1].

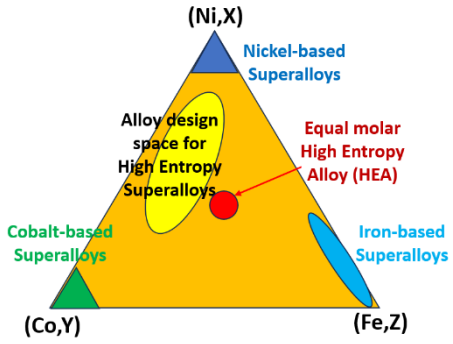

(a)

(b)

Fig. 2. (a) Space for High Entropy Alloy and Property comparison with Nickel-Based superalloy (Tsao 2017) and (b) classification of alloys based on their configurational entropy [9].

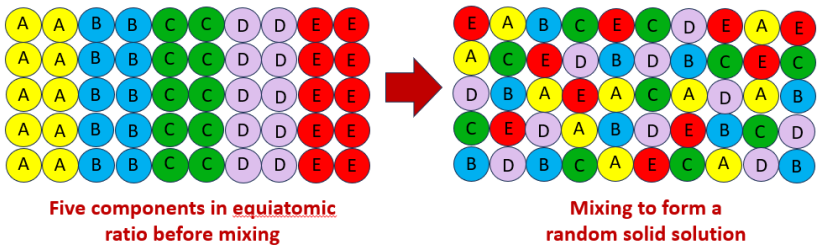

Fig. 3. Schematic formation of a disordered single-phase solid solution in HEA [15].

Early studies of HEA have revealed that most HEAs have disordered single-phase solid solutions, as schematically depicted in Fig. 6, of either FCC, HCP, or BCC. With such structures, these alloys have been reported to exhibit outstanding properties such as high strength, low density, high oxidation resistance, and high microstructural stability due to low diffusion and lower cost [17,18]. Based on the configurational entropy, alloys are classified as high entropy, medium entropy, and low entropy alloys. Examples of low entropy alloys are mild steels, while stainless steels and superalloys are medium entropy alloys.

High-temperature applications of alloys require a protective oxide layer with specific properties such as thermodynamic stability, kinetic slow rate of formation, and strong adhesion to the substrate. Oxides of Al_2O_3 and Cr_2O_3 are normally selected for high-temperature corrosion of engineering alloys, as the Ellingham diagram of oxide formation indicates that they are relatively stable. Oxide formation during isothermal oxidation usually follows a parabolic rate law, conventional alloys, where one particular element dominates in the alloy composition, such as Ni-based, Fe-based, or Co-based superalloys, the HEAs contain at least five relatively equimolar metal elements as schematically shown in **Error! Reference source not found.**. Based on the configurational entropy, ΔS_{config}, defined in Equation 1, this group of alloys should have at least 1.5R (see **Error! Reference source not found.**), where R is the gas constant, n is the number of elements, and X_i is the mole fraction of elements.

$$\Delta S_{conf} = -R \sum_{i=1}^{n} x_i \ln(x_i) \quad (1)$$

A new concept of alloy systems called High Entropy Alloy (HEA) was proposed separately by Cantor [2] and Yeh [15] about two decades ago. Unlike the concept of indicating that the oxide scale formation is controlled by diffusion of ions along the scale thickness.

From a kinetic point of view, Fig. 4 shows that Al_2O_3 has the lowest parabolic rate constant among those three two oxides, so this scale is normally selected for protecting alloys against high-temperature oxidation. Cr_2O_3 is only stable at temperatures below 1000°C because it is further oxidized to form volatile CrO_3, but it has excellent hot corrosion resistance at temperatures below 1000°C. To increase the adherence resistance of the scale, small amounts (dopant) of reactive elements such as Y, Hf, Ce, and Zr are normally added to high-temperature alloys.

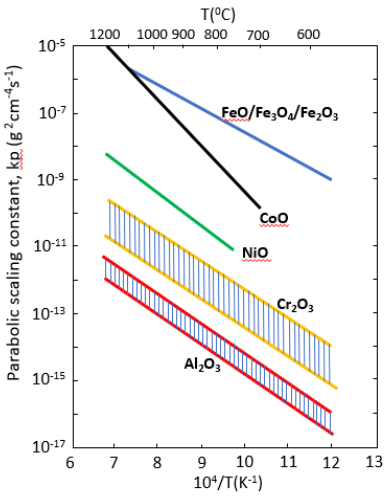

Fig. 4. Parabolic oxidation rate constant, k_p, for the growth of various oxide scales as a function of temperature [4].

2 EXPERIMENTAL WORKS

Two different HEAs of $Al_{0.75}CoCrFeNi$ and $Al_{0.75}CoCuCrFeNi$ were prepared by melting the calculated and weighed pure elements of Al, Cr, Fe, Ni, Co, and Cu in a single electrode arc furnace purged with high-purity argon. The button ingots were melted four times and further treated for homogenization by heating at 1100°C for 10 h. The homogenized buttons were then cut into several coupons for microstructural analysis and high-temperature oxidation simulations. Isothermal oxidation tests were performed by heating the coupons at 800, 900, 1000, and 1100°C for 2, 16, 40, and 168 h. in a tube furnace under an air atmosphere. The weight change of each sample was measured, and both the oxidized and homogenized alloy samples were characterized using an X-ray diffraction (XRD) instrument (SmartLab, Rigaku, Tokyo, Japan) and a scanning electron microscope (SEM) equipped with an energy-dispersive spectroscopy (EDS) analyzer was attached (JCM-7000 Neoscope™, JEOL, Tokyo, Japan). An etching solution containing 1.5% HNO_3 – 2.5% H_2SO_4 - 46% HCl - 50% ethanol was used to reveal the microstructures of the alloys.

3 RESULTS AND DISCUSSION

3.1 Phase Prediction for High Entropy Alloys

Several methods have been developed to predict the phases that occur in the microstructures of HEAs, such as thermodynamic calculation, the Hume-Rothery rule, and the electron valence parameter. Based on the Hume-Rothery rule, the difference in atomic radius (δ), and the enthalpy of mixing (ΔH_{mix}) are the main factors in the phase prediction of HEAs [9]. The following equation can be used to calculate the difference in atomic radius.

$$\delta = \sqrt{\sum_{i=1}^{N} c_i \left(1 - \frac{r_i}{\sum_{i=1}^{N} c_i r_i}\right)^2} \qquad (2)$$

where r_i is the atomic radii of element "i" while C is the concentration of the element "i" in the alloy system. The radii of the element is the Goldshmidt radii which is the radii of an element when the coordination number is 12 [5,8]. The enthalpy of mixing of the multi-component systems can be calculated using the following equation.

$$\Delta H_{mix} = \sum_{i=1}^{N} \Delta H_{ij}^{mix} c_i c_j \qquad (3)$$

The ΔH_{ij}^{mix} variable is the enthalpy of mixing for a binary system of elements i and j, while C_i is the concentration of i in atomic percent. To determine the type of phases that occur in HEAs, either in the form of solid solution, amorphous, or intermetallic compound, the values of ΔH_{mix} and δ are then plotted in Fig. 5.

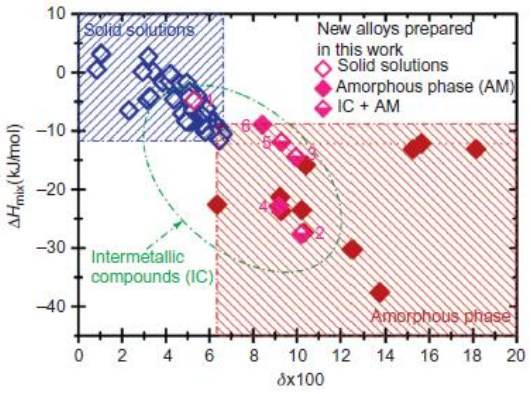

Fig. 5. Different types of phases occur in HEAs, either solid solution, amorphous, or intermetallic, based on ΔH_{mix} and δ values [9].

Guo et al [5] have proposed a method to predict the crystal structures, either FCC or BCC, of phases that occur in HEAs, using a parameter known as valence electron concentration (VEC) as follows.

$$VEC = \sum C_i(VEC_i) \qquad (4)$$

Where C is the concentration of elements in the alloy. When the VEC is less than 6.8, the alloy tends to form a BCC phase, while when the VEC is higher than 8 FCC, the phase is FCC. The duplex structure of FCC and BCC would occur in the HEAs when the VEC value is in the range of 6.8-8. An illustration of this phase prediction method in HEAs is given for $Al_{0.75}CoCrFeNi$ alloy. This material has a VEC of 7.42 and therefore the alloy should have a solid solution containing two phases of FCC and BCC crystal structure. It was found that the δ value of $Al_{0.75}CoCrFeNi$ is 5.29% and the ΔH_{mix} is -10.90 KJ/mol. From Fig. 5, it is predicted that the alloy has a duplex microstructure containing solid solution and intermetallic compound phases. However, since the phase diagrams of the $Al_{0.75}CoCrFeNi$ and $Al_{0.75}CoCrCuFeNi$ alloys are available in the literature, these two HEAs would be used to analyze the microstructures of the alloys, as given in subchapters 3.3 and 3.5.

3.2 Metal Loss During Melting

In practice, it is difficult to avoid metal loss during melting. This metal loss occurs due to several mechanisms, mainly oxidation and evaporation. Metal loss can be minimized by using a vacuum atmosphere or an inert gas, such as argon. In our experiments, melting was conducted using a single-electrode DC arc furnace with high-purity argon purging. Evaluation of the chemical composition change of the alloys should be done to have the real configurational entropy of the alloy. In this paper, an example effort to evaluate the configurational entropy of the alloy after melting and homogenization is taken from the $Al_{0.75}$CoCrFeNi alloy. The initial chemical composition of $Al_{0.75}$CoCrFeNi alloy is shown in Table 1. After melting and homogenization, the chemical composition of the button was analyzed using EDS in the SEM because the coupon was too small for spectroscopic analysis. Fig. 6 shows the result of the EDS analysis showing the change in chemical composition. It can be seen that Al has decreased from 15.79 to 12.45% while other elements have increased. Even though the melt was protected by high-purity argon, the low oxygen content in the furnace atmosphere still oxidized the elements, mostly aluminum. Some inclusions remaining in the alloy are shown in Fig. 7. The effect of oxidation during homogenization was neglected because only the surface of the button was slightly oxidized while the center of the button was unaffected. Examination of the entropy configuration of the homogenized alloy indicated that the alloy has a ΔS_{config} of 1.589R, which is higher than 1.5R. Therefore, the alloy still has high entropy properties after melting and homogenization.

Table 1. Chemical composition and mass of each element for $Al_{0.75}$CoCrFeNi alloy making before melting.

Element	% atom	Mass (gr)
Al	15.79	1.6471
Cr	21.05	4.2327
Fe	21.05	4.5452
Ni	21.05	4.7788
Co	21.05	4.7770
Total	100	19.9808

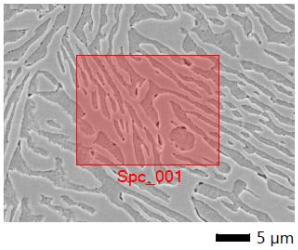

Element	Line	Mass%	Atom%
Al	K	6.37±0.15	12.45±0.29
Cr	K	20.88±0.36	21.19±0.37
Fe	K	23.21±0.48	21.92±0.45
Co	K	24.60±0.57	22.02±0.51
Ni	K	24.95±0.63	22.42±0.57
Total		100.00	100.00
Spc_001			Fitting ratio 0.0461

Fig. 6. EDS analysis of the homogenized $Al_{0.75}$CoCrFeNi alloy.

3.3 Microstructures of $Al_{0.75}$CoCrFeNi alloy

The microstructures of the homogenized $Al_{0.75}$CoCrFeNi alloy are shown in Fig. 7 and Fig. 8, for backscattered and secondary electron images, respectively. The alloy has a lamellar-type microstructure consisting of the A1-FCC phase and the B2-BCC phase. However, between lamellas of these two phases, it was found that black spots were observed in the back-scattered images (Fig. 7), which was further confirmed as pores in the secondary electron images (Fig. 8). It is expected that these pores were previously other BCC phase particles that were dissolved during etching leaving pores. EDS analysis was unable to confirm these pores, so further analysis was required to confirm these microconstituents. However, using the phase diagram of the high-entropy alloy Al_xCoCrFeNi constructed using the CALPHAD method done by Zhang, at 1100°C the Al_xCoCrFeNi should have three phases, *i.e.*, FCC phase, A2 BCC phase, and B2 BCC phase, as shown in Fig. 9.

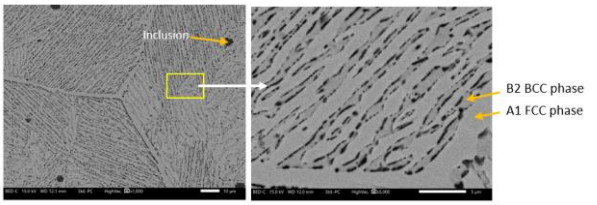

Fig. 7. Backscattered electron images of $Al_{0.75}$CoCrFeNi alloy microstructure.

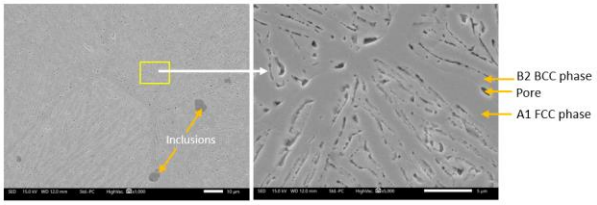

Fig. 8. Secondary electron images showing the microstructure of $Al_{0.75}$CoCrFeNi alloy.

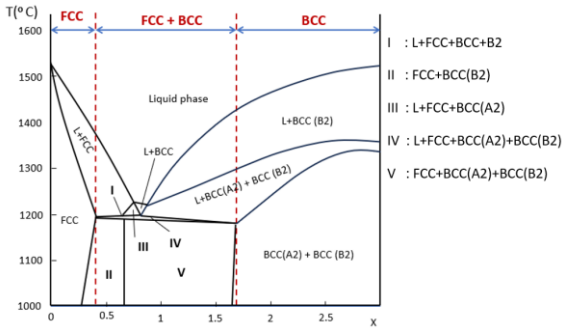

Fig. 9. Phase diagram of the high-entropy alloy Al_xCoCrFeNi constructed using the CALPHAD method [16].

3.4 Microstructures of $Al_{0.75}$CoCrCuFeNi alloy

The addition of copper in the Al_xCoCrFeNi significantly changes the microstructure of the HEAs. Using equation 2 the misfit (δ) of the $Al_{0.75}$CoCrCuFeNi is 0.0417 or 4.17%. Meanwhile, the mixing enthalpy (ΔH_{mix}) of the alloy is -2.57kJ/mol indicating that the alloy tends to form a solid solution and intermetallic compound. The stable phases in $Al_{0.75}$CoCrCuFeNi alloy at 1100°C can

be predicted from the phase diagram of $Al_xCoCrCuFeNi$ with variation in Al content as shown in Fig. 10. Based on this phase diagram, the alloy is predicted to have two phases containing FCC phase and BCC phase. The FCC phase is considered a random solid solution matrix of the alloy, while the BCC phase is an ordered intermetallic phase of typically aluminide compounds.

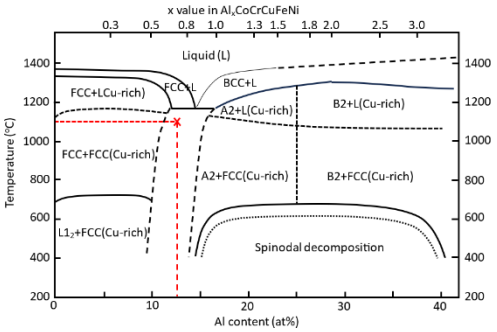

Fig. 10. Phase diagram of $Al_xCoCrCuFeNi$ with a variation of Al content [12].

Fig. 11 shows the elemental mapping and EDS analysis of different areas on the microstructures of $Al_xCoCrCuFeNi$ alloy. It is seen that the matrix, represented by a bright area, has a chemical composition indicated by area 02 in the table. This phase is believed to have a random solid solution with FCC. Meanwhile, there are certain areas, shown SEM micrograph as well as the x-ray mapping that contain small particles rich in nickel and aluminum. These particles are expected as the B2-ordered intermetallic compound of typically aluminide M_xAl_y, where M are metals of either Ni, Fe, or Co, as indicated by area 06 in the table. The black areas are expected to shrinkage voids that are surrounded by a phase rich in copper as shown by area 05. The alloy of $Al_xCoCrFeNi$ copper has very small solubility and during solidification of $Al_{0.75}CoCrCuFeNi$ alloy the copper atoms segregate along the grain boundaries and it gives shrinkage voids when complete solidification has been reached.

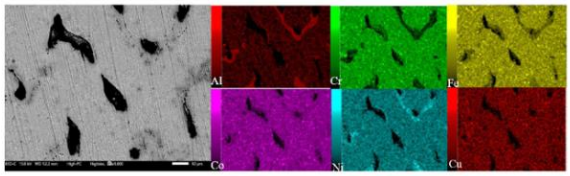

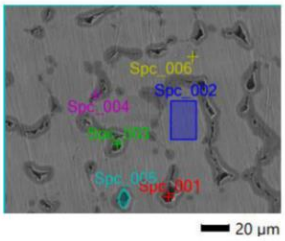

Element	Chemical composition of areas (at.%)					
	01	02	03	04	05	06
Al	6.16	8.61	6.73	6.04	1.69	61.35
Cr	26.19	21.74	23.93	39.12	7.51	8.16
Fe	20.39	22.45	23.32	21.34	6.35	8.84
Co	22.21	22.34	22.32	18.12	6.39	9.37
Ni	18.97	17.96	17.50	12.68	9.91	10.41
Cu	6.09	6.89	6.19	2.70	68.14	1.87

Fig. 11. Elemental mapping and EDS analysis of different areas on the microstructures of $Al_{0.75}CoCrCuFeNi$ alloy

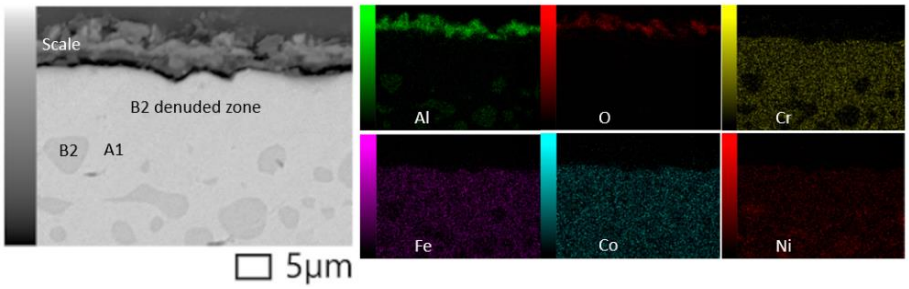

Fig. 12. Microstructure and elemental x-ray mapping of $Al_{0.75}CoCrFeNi$ alloy oxidized at 1100°C for 40 hrs.

3.5 High-Temperature Oxidation Behavior of HEAs

Oxidation of the $Al_{0.75}CoCrFeNi$ alloy at 900, 1000, and 1100°C gave scales consisting of an external layer of alumina. **Error! Reference source not found.** shows the x-ray mapping of the cross-section of the sample oxidized at 1100°C for 40 hrs. It is therefore concluded that $Al_{0.75}CoCrFeNi$ alloy has relatively high isothermal oxidation resistance. Nevertheless, the adherent resistance of this alloy has not been well studied and further cyclic oxidation simulation needs to be carried out.

The isothermal oxidation of $Al_{0.75}CoCrCuFeNi$ alloy 900, 1000, and 1100°C showed different oxidation behavior compared with that of $Al_{0.75}CoCrFeNi$. An external layer of Al_2O_3 was not significantly observed, but Cr_2O_3 was more dominant, as shown by the XRD patterns depicted in Fig. 13. Fig. 14 shows the microstructure and elemental x-ray mapping of $Al_{0.75}CoCrCuFeNi$ alloy oxidized at 1100°C for 40 hrs. This scale is relatively much thicker compared with the scale found in $Al_{0.75}CoCrFeNi$ (**Error! Reference source not found.**). Besides chromium, the scale contains other oxides and spinel as shown by the XRD

patterns. The copper oxide was found in the scale as shown in
Fig. **15**.

Fig. **16** shows the plot between weight gain and times after oxidation simulation of the $Al_{0.75}CoCrCuFeNi$ alloy. When curve fittings and regressions for three possible behaviors, *i.e.,* linear, logarithmic, and parabolic, it is found that the rate behavior of the $Al_{0.75}CoCrCuFeNi$ alloy is parabolic. The rate constants (K_p) for 900, 1000, and 1100°C are 3.84 x 10^{-10}, 5.99 x 10^{-10}, and 8.97 x 10^{-10} (mg/cm^2.s), respectively. These values are considered relatively low when the Kps of pure elements given in Fig. 4 are considered, which are close to the values for the oxidation of chromium. When a plot between ln K_p vs. 1/T was made, the activation energy for the formation of oxide scale on $Al_{0.75}CoCrCuFeNi$ alloy is 66.58 kJ/mol, which is relatively low when compared with superalloys [7].

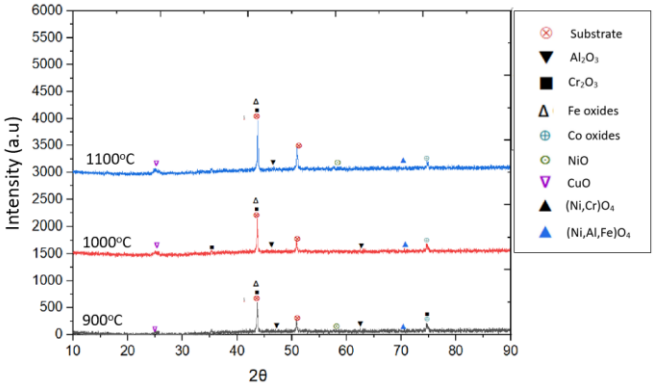

Fig. 13. X-ray diffraction patterns of $Al_{0.75}CoCrCuFeNi$ alloy oxidized at 900, 1000, and 1100°C for 40 hrs

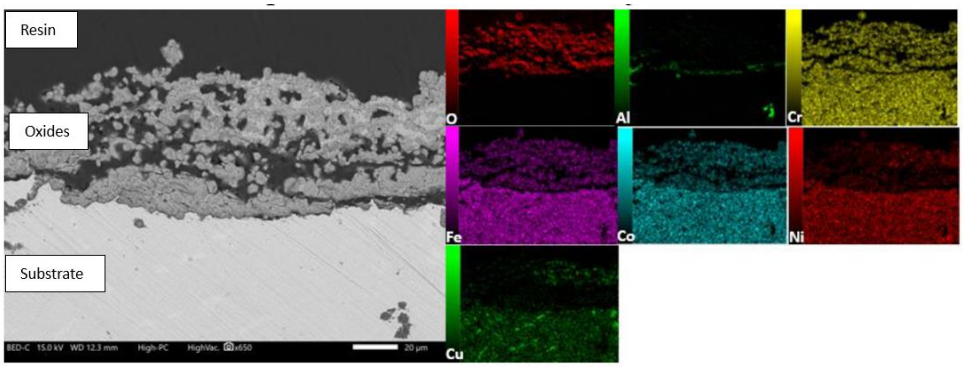

Fig. 14. Microstructure and elemental x-ray mapping of $Al_{0.75}CoCrCuFeNi$ alloy oxidized at 1100°C for 40 hrs.

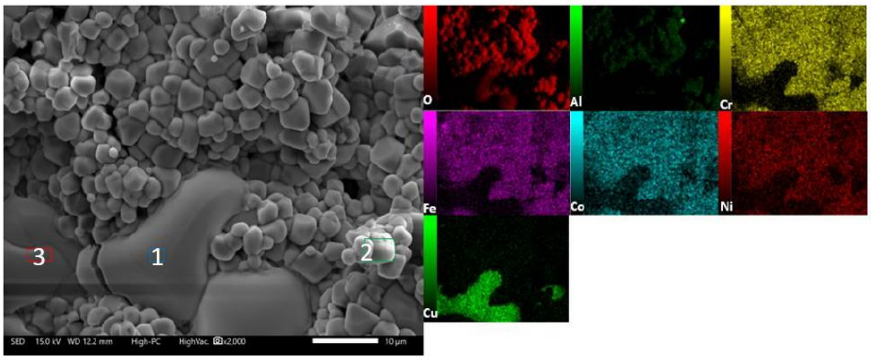

Area	Chemical composition (at.%)						
	O	Al	Cr	Co	Cu	Fe	Ni
1	50.75	0.57	0.85	1.5	44.66	0.73	0.94
2	53.23	9.92	10.57	7.69	4.26	8.86	5.49
3	11.32	1.93	4.69	5.59	70.31	3.43	2.74

Fig. 15. Morphology of the oxide scale on the surface of $Al_{0.75}CoCrCuFeNi$ alloy oxidized at 1100°C for 40 hrs. and EDS results of certain areas.

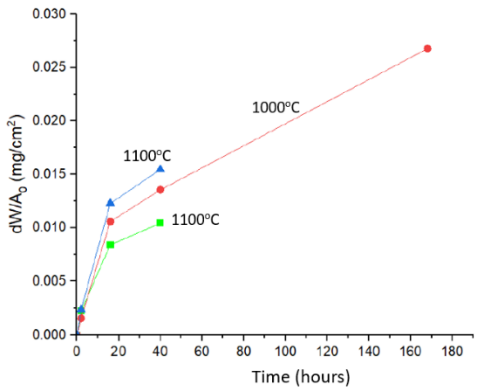

Fig. 16. Weight gains when $Al_{0.75}CoCrCuFeNi$ alloy oxidized at 900, 1000, and 1100°C for various times. Note: only oxidation at 1000ºC was carried out up to 168 hrs. (7 days).

4 Conclusions

The study on microstructural analysis and high-temperature oxidation of high entropy alloys showed that based on the results obtained from the high-temperature isothermal oxidation experiments on $Al_{0.75}CoCrFeNi$ and $Al_{0.75}CoCrCuFeNi$ alloys have revealed some findings as follows. The addition of Cu on $Al_{0.75}CoCrFeNi$ alloy changed the microstructures from lamellar duplex structure of A1 FCC and B2 BCC to dendritic matrix of FCC and B2 BCC precipitates preferentially dispersed around the grain boundaries, while copper-rich phases were formed around shrinkage voids in the interdendritic regions. If the $Al_{0.75}CoCrFeNi$ alloy formed an oxide scale with an external layer dominated by Al_2O_3, the $Al_{0.75}CoCrCuFeNi$ alloys formed an oxide scale containing mostly Cr_2O_3 with small amounts of spinel and copper oxide (CuO). The scale is porous, indicating that it is not protective. The oxidation behavior of both alloys follows a parabolic rate, indicating that the scale is controlled by the diffusion of ions in the formed oxide. The oxidation rate constants for $Al_{0.75}CoCrCuFeNi$ oxidized at 900, 1000, and 1100°C are 3.84 x 10^{-10}, 5.99 x 10^{-10}, and 8.97 x 10^{-10} ($mg/cm^2.s$), respectively, with activation energy for oxidation of 66.58 kJ/mol.

Acknowledgments The authors are grateful for the financial support from the Program Riset dan Inovasi untuk Indonesia Maju (RIIM) Gelombang 2 the National Research and Innovation Agency (BRIN) and LPDP, grant number 78/IV/KS/11/2022 and 834/IT1.B07/KS.00/2022. The authors would like to acknowledge the support from PT Gunbuster Nickel Industry for providing the SEM-EDS (JCM-7000 NeoScope™, JEOL, Tokyo, Japan) used for the analysis of the samples in this work.

References

1. Basuki, E.A, Crosky, A., "Microstructural Changes in Overheated Nickel-Base Superalloys. Proceedings of The Conference on Microscopy: Materials and Techniques, Institute of Metals and Materials Australia Ltd., Mascot, New South Wales, Australia, 21-22 September 1993.
2. Cantor B, Chang ITH, Knight P, Vincent AJB. Microstructural development in equiatomic multicomponent alloys. Materials Science and Engineering A 2004;375–377:213–8. https://doi.org/10.1016/j.msea.2003.10.257.
3. Chen, Y.T., Vhang, Y.J., Murakami, H., Gorsse, S., Yeh, A.C., Designing high entropy superalloys for elevated temperature application, Scripta Materalia, 187, 2020.
4. Gleeson, B., High-Temperature Corrosion of Metallic Alloys and Coatings, Materials Science and Technology, Cahn, R.W, Haasen, P., and Kramer, E.J. (Eds), Chapter-April 2008. DOI: 10.10002/9783527619306.ch14.
5. Guo, S., & Liu, C. T. (2011). Phase stability in high entropy alloys: Formation of solid-solution phase or amorphous phase. Progress in Natural Science: Materials International, 21(6), 433–446. doi:10.1016/s1002-0071(12)60080-x
6. Heilmaier M, Krüger M, Saage H, Rösler J, Mukherji D, Glatzel U, et al. Metallic materials for structural applications beyond nickel-based superalloys. JOM 2009;61:61–7. https://doi.org/10.1007/s11837-009-0106-7.
7. Ma, S., Ding, Q., Wei, X., Zhang, Z., Bei, H., The effect of alloying element Cr, Al and Si on oxidation behaviors of Ni-based superalloys, Materials MDPI, 2022, 15, 7352, https://doi.org/10.3390/ma15207352.
8. Miracle DB, Senkov ON. A critical review of high entropy alloys and related concepts. Acta Mater 2017;122:448–511. https://doi.org/10.1016/j.actamat.2016.08.081.
9. Murty BS. High-entropy alloys. Butterworth-Heinemann; 2014.
10. Pollock TM, Tin S. Nickel-Based Superalloys for Advanced Turbine Engines: Chemistry, Microstructure and Properties. J Propuls Power 2006;22:361–74. https://doi.org/10.2514/1.18239.
11. Stroosnijder MF, Mévrel R, Bennett MJ. The interaction of surface engineering and high temperature corrosion protection. Materials at High Temperatures 1994;12:53–66. https://doi.org/10.1080/09603409.1994.11689470.
12. Tong, C.-J., Chen, M.-R., Yeh, J.-W., Lin, S.-J., Chen, S.-K., Shun, T.-T., & Chang, S.-Y. (2005). Mechanical performance of the Al x CoCrCuFeNi high-entropy alloy system with multiprincipal elements. *Metallurgical and Materials Transactions A*, *36*(5), 1263–1271. https://doi.org/10.1007/s11661-005-0218-9.
13. Tsao, T.K., Yeh, A.C., Kuo, C.M, Kakehi, K., Murakami, H., Yeh, J.W., Jian, S.R., The high temperature tensile and creep behaviors of high entropy superalloys, Science Report, 7, 2017.
14. Xia W, Zhao X, Yue L, Zhang Z. A review of composition evolution in Ni-based single crystal superalloys. J Mater Sci Technol 2020;44:76–95. https://doi.org/https://doi.org/10.1016/j.jmst.2020.01.026.
15. Yeh JW, Chen SK, Lin SJ, Gan JY, Chin TS, Shun TT, et al. Nanostructured high-entropy alloys with multiple principal elements: Novel alloy design concepts and outcomes. Adv Eng Mater 2004;6:299–303. https://doi.org/10.1002/adem.200300567.
16. Zhang Y, Zuo TT, Tang Z, Gao MC, Dahmen KA, Liaw PK, et al. Microstructures and properties of high-entropy alloys. Prog Mater Sci 2014;61:1–93. https://doi.org/https://doi.org/10.1016/j.pmatsci.2013.10.001
17. O. N. Senkov, G. B. Wilks, D. B. Miracle, C. P. Chuang, and P. K. Liaw, "Refractory high-entropy

alloys," Intermetallics, vol. 18, no. 9, pp. 1758–1765, 2010, doi: 10.1016/j.intermet.2010.05.014.
18. M. A. Hemphill et al., "Fatigue behavior of Al0.5CoCrCuFeNi high entropy alloys," Acta Mater., vol. 60, no. 16, pp. 5723–5734, 2012, doi: https://doi.org/10.1016/j.actamat.2012.06.046